ЖЭТФ, 2024, том 165, вып. 4, стр. 536–543

FERROMAGNETIC RESPONSE OF THIN NiI_2 FLAKES UP TO ROOM TEMPERATURES

N. N. Orlova, A. A. Avakyants, A. V. Timonina, N. N. Kolesnikov, E. V. Deviatov*

Yu. A. Osipyan Institute of Solid State Physics of the Russian Academy of Sciences 142432, Chernogolovka, Moscow District, Russia

Received November 14, 2023,
revised version January 23, 2024
Accepted for publication January 24, 2024

We investigate the magnetic response of thin NiI_2 flakes for temperatures above 80 K. Since no magnetic ordering is expected for bulk NiI_2, we observe clear paramagnetic response for massive NiI_2 single crystals. In contrast, thin NiI_2 flakes show well-defined ferromagnetic hysteresis loop within ± 2 kOe field range. The value of the response does not scale with the sample mass, ferromagnetic hysteresis can be seen for any flake orientation in the external field, so it originates from the sample surface, possibly, due to the anisotropic exchange (Kitaev interaction). The observed ferromagnetism is weakly sensitive to temperature up to 300 K. If a flake is multiply exposed to air, ferromagnetic hysteresis is accompanied by the periodic modulation of the magnetization curves, which is usually a fingerprint of the multiferroic state. While NiI_2 flakes can not be considered as multiferroics above 80 K, surface degradation due to the crystallohydrate formation decreases the symmetry of NiI_2 surface, which produces the surface ferroelectric polarization in addition to the described above ferromagnetic one.

DOI: 10.31857/S0044451024040084

1. INTRODUCTION

Recent interest to multiferroics is mostly connected with layered van der Waals materials and van der Waals heterostructures [1]. In the simplest case, multiferroic heterostructure is composed from alternating ferroelectric and ferromagnetic monolayers [2, 3]. Multiferroic state has also been predicted theoretically for layered van der Waals single crystals [4]. Experimentally, multiferroic properties have been demonstrated for some dihalides (MX_2, X = Cl, Br, I) like CrI_2 [5], MnI_2 [6], CoI_2 and NiI_2 [7, 8].

Among these materials, NiI_2 is characterized [7] by one of the highest transition temperatures T_{N2}= 59.5 K. It is also known as type-II multiferroic [4], where ferroelectricity can only appear in the specific magnetically ordered state [9]. For NiI_2, the structural transformation to monoclinic noncentrosymmetric lattice is accompanied by transition to a helimagnetic state that displays finite electric polarization [7, 8, 10, 11].

It is surprising that multiferroic state can survive down to monolayers [12]. Electromagnetic multiferroicity was confirmed in few layers and monolayers of NiI_2, which makes it the first established two-dimensional multiferroic [8, 12]. While decreasing the crystal thickness to monolayers, symmetry requires appropriate changes in the ground state and, therefore, the transition temperature T_{N2}. To explain the helical ground state in the monolayer NiI_2, Kitaev interaction [13–15] and a biquadratic term [16] have recently been proposed [17]. For monolayer samples, T_{N2} is found [8, 12] to be decreased to 21 K. The transition temperature is monotonically increasing with number of layers, so it is 41 K for the four-layer samples [8, 12], 58 K for the 60-layer ones [18], which is close to the bulk value [7] T_{N2}= 59.5 K. Thus, a 100-layer sample should be regarded as a massive single crystal for its multiferroic properties.

While the multiferroic state appears below T_{N2}, the magnetic ordering is known even at higher temperatures [7, 8]. Bulk NiI_2 shows [19] interlayer antiferromagnetic and intralayer ferromagnetic orders below T_{N1}=76 K. In contrast to T_{N2}, the ordering tempera-

* E-mail: dev@issp.ac.ru

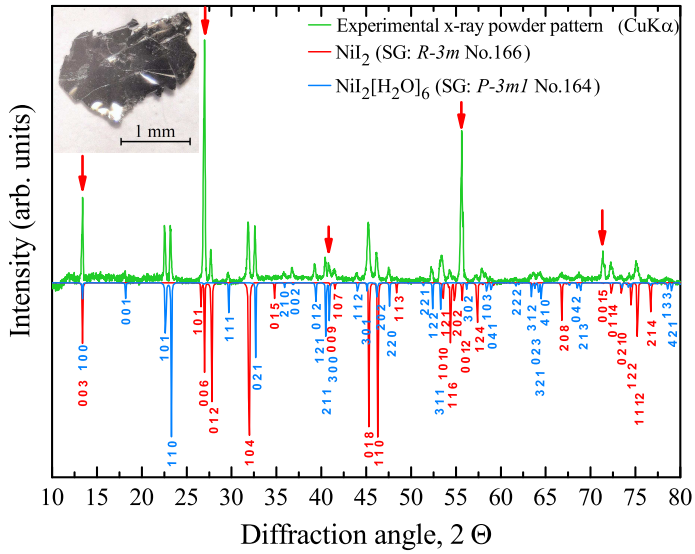

Fig. 1. (Color online) The powder X-ray diffraction analysis of NiI_2 single crystals. The experimental X-ray powder pattern is shown by the green curve. The model X-ray diffraction patterns of pure NiI_2 and $NiI_2[H_2O]_6$ phases are shown by red and blue curves, respectively. Analysis confirms the known NiI_2 structure with trigonal syngony $R\bar{3}m$ (space group No.166, $CdCl_2$ prototype) with some admixture of nickel iodide hexahydrate phase, see the text. The data are obtained at room temperature. Intensity of the diffraction peaks shows distinct texture due to the (001) plane (red arrows), which well corresponds to the layered NiI_2 single crystal structure. Inset: optical image of a large single crystal flake, which also shows NiI_2 layers

ture T_{N1} is predicted [20] to increase in monolayers up to 178 K, while the type of magnetic ordering is still debatable [21, 22]. In general, Kitaev exchange term, when combined with magnetic frustration, can lead to an emergent chiral interaction, which is also responsible for topological spin structures [13].

Experimental investigation of the magnetic response for NiI_2 monolayers is seriously complicated by known NiI_2 degradation due to the crystallohydrate formation [18]. On the other hand, theoretical consideration on symmetry and Kitaev interaction should be also valid for NiI_2 surface. The surface-defined magnetic response can be dominant for the thin flakes, which are more accessible for direct magnetic investigations than monolayers.

Here, we investigate the magnetic response of thin NiI_2 flakes for temperatures above 80 K. Since no magnetic ordering is expected for bulk NiI_2, we observe clear paramagnetic response for massive NiI_2 single crystals. In contrast, thin NiI_2 flakes show well-defined ferromagnetic hysteresis loop within ± 2 kOe field range. The value of the response does not scale with the sample mass, ferromagnetic hysteresis can be seen for any flake orientation in the external field, so it originates from the sample surface, possibly, due to the anisotropic exchange (Kitaev interaction).

2. SAMPLES AND TECHNIQUES

NiI_2 single crystals were grown by iodine transport in the evacuated silica ampule. The initial load consisted of the mixture of nickel ($15\times1\times0.5$ mm^3 nickel foil stripes, 99.9%) and iodine (99.5%), taken in the stoichiometric ratio. The ampule was placed in the two-zone furnace, the load zone was kept at 700°C while the growth zone was cooled to 550°C. The distance between the zones was 150 mm. The obtained NiI_2 single crystals are of layered structure, see the image in the inset to Fig. 1. NiI_2 composition and structure are verified by energy-dispersive X-ray spectroscopy and X-ray diffraction analysis, respectively.

NiI_2 is characterized by degradation in ambient conditions [18] due to the crystallohydrate formation. In our experience, 20 μm thick flake obtains characteristic cyan color [23] for about 5 hours in air. However, crystallohydrate appears on the flake surface even for the short air depositions, e.g. while the flake is transferred to the sample holder, see the X-ray diffraction pattern in Fig. 1.

The powder X-ray diffraction analysis confirms the main NiI_2 phase with some admixture of nickel iodide hexahydrate phase, as depicted in Fig. 1. The known NiI_2 structure with trigonal syngony $R\bar{3}m$ (space group No.166, $CdCl_2$ prototype) is confirmed. Intensity of

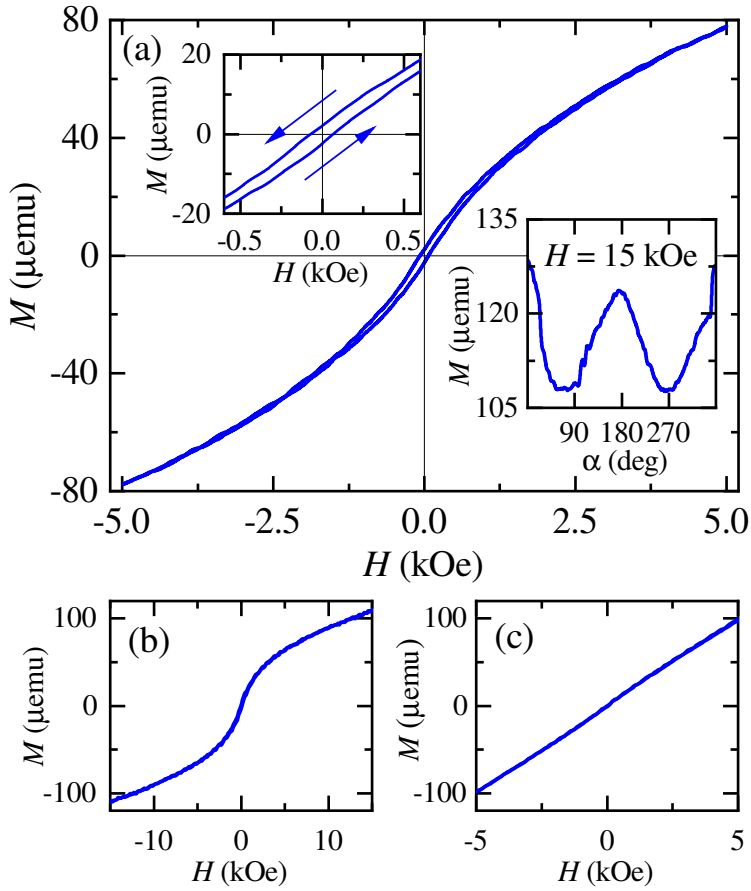

Fig. 2. (Color online) Magnetization behavior of NiI_2 flakes for the side mount orientation, α is the angle between the flake surface and the magnetic field. The data are obtained at 120 K temperature. a — Ferromagnetic hysteresis for the 18 μm thick, 0.23 mg mass flake, magnetic field is parallel to the flake surface, $\alpha = 0$. The hysteresis is observed within ± 2 kOe field range. For clarity, the central region is enlarged in the left inset. Right inset shows typical ferromagnetic anisotropy of magnetization in high fields (15 kOe), $M(H)$ is diminished for normal field orientation, $\alpha = 90^\circ$. b — $M(H)$ curves in a wide field range, $\alpha = 90^\circ$. Outside the hysteresis region ± 2 kOe, $M(H)$ shows linear paramagnetic dependence. c — Magnetization curves for a massive sample (100 μm, 0.88 mg). The linear dependence shows clear paramagnetic response, as it should be expected [19, 20] for bulk NiI_2 at temperatures above $T_{N1} = 76$ K

the diffraction peaks shows distinct texture due to the (001) plane, which well corresponds to the layered NiI_2 single crystal structure. The data are obtained at room temperature, while this NiI_2 structure is known to survive [10, 11] until 59.5 K. Below 59.5 K, the structure is monoclinic, due to a slight distortion from the C-centered lattice [24]. Thus, the performed X-ray diffraction analysis certainly valid in our temperature range 80–300 K.

Since we can not avoid surface degradation completely, we should control it by definite sample handling. The initial bulk NiI_2 single crystal is stored in vacuum in the sealed ampule. After opening to air, an exfoliated flake is immediately placed in the nitrogen flow cryostat and cooled down to 80 K. The residual part of the initial NiI_2 single crystal is stored in liquid nitrogen. The second sample is obtained by warming it to the room temperature in the flow of dry nitrogen, mechanical exfoliation of a thin flake, and cooling down the NiI_2 single crystal again. Despite the all precautions, the next sample is always more corrupted than the previous one, which allows to control possible crystallohydrate effects.

We investigate magnetic response of thin NiI_2 flakes by Lake Shore Cryotronics 8604 VSM magnetometer equipped with nitrogen flow cryostat. A flake is mounted to the magnetometer sample holder by low temperature grease, which has been tested to have a negligible magnetic response. The flake's surface can be rotated in magnetic field both for the side mount

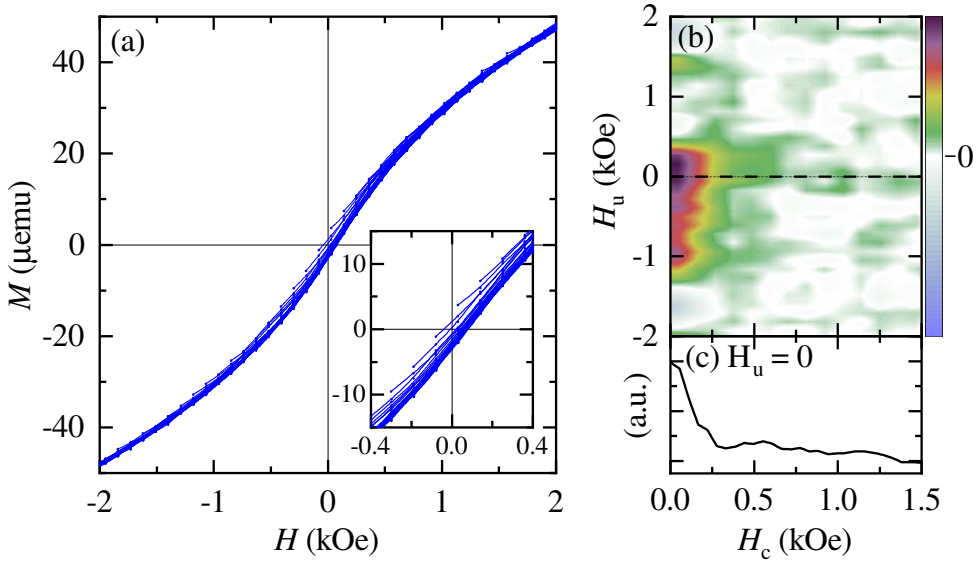

Fig. 3. (Color online) FORC analysis for the same 18 μm thick, 0.23 mg mass flake as in Fig. 2. a — Raw FORC data, obtained as multiple magnetization $M(H, H_r)$ curves [25,26]. Before every curve, the magnetization is stabilized at fixed positive saturation field $H_s = 2$ kOe. The starting reversal field H_r is gradually shifted to the lower fields. The data are obtained at 120 K. Magnetic field is parallel to the flake surface, $\alpha = 0$. Inset shows the enlaged region within ± 2 kOe field range. b — The calculated FORC density diagram, where $H_u = \frac{1}{2}(H + H_r)$ is known as the interaction field and $H_c = \frac{1}{2}(H - H_r)$ is the coercive field. Single peak in $\rho(H_u, H_c)$ and the so-called open contours at the H_u axis are usually regarded as a fingerprint of the multidomain ferromagnet [27,28]. c — Scan of the FORC density along $H_u = 0$ line in (b)

case in Figs. 2, 4, 5 a, and for the top mount orientation in Fig. 5 b. In the every case, we perform centering and saddling procedures to establish the correct sample position in the magnetometer.

We investigate sample magnetization by standard method of the magnetic field gradual sweeping between two opposite saturation values to obtain hysteresis loops at different temperatures. Apart from the hysteresis measurements, we perform first order reversal curve (FORC) analysis [25,26], which is of growing popularity nowadays. The raw FORC data are obtained as multiple magnetization $M(H, H_r)$ curves [25, 26]. Before every curve, the magnetization is stabilized at fixed positive saturation field H_s. As a second step, the field is changed to the chosen reversal field H_r, so the $M(H)$ curve can be recorded toward the positive saturation field H_s. For the next FORC curve, the starting reversal field H_r is shifted to the lower magnetic field. The FORC density distribution $\rho = (-1/2)(\partial^2 M(H, H_r)/\partial H \partial H_r)$ is calculated by standard Lake Shore Cryotronics software. Here, $H_u = \frac{1}{2}(H + H_r)$ is known as the interaction field and $H_c = \frac{1}{2}(H - H_r)$ is the coercive field. FORC analysis provides information on the magnetization reversal, which can not be obtained from standard hysteresis loops [27,28].

3. EXPERIMENTAL RESULTS

Fig. 2 a shows typical magnetization behavior of NiI_2 thin flakes. To our surprise, 18 μm thick, 0.23 mg mass flake demonstrates clear ferromagnetic hysteresis even at 120 K, i.e. well above the bulk T_{N1}=76 K. We also observe typical ferromagnetic anisotropy of magnetization, see the right inset to Fig. 2 a. This anomalous hysteresis is enlarged in the left inset to Fig. 2 a, it appears within ± 2 kOe field range. In higher fields, $M(H)$ is of the linear paramagnetic behavior, as depicted in Fig. 2 b.

In contrast, massive samples show clear paramagnetic response, as it should be expected from previous publications [19, 20], see Fig. 2 c for the 100 μm thick, 0.88 mg mass flake. It is important that $M(H)$ values at 15 kOe does not scale with the sample mass in Fig. 2 a and c, so the ferromagnetic response might be attributed to the flake surface.

The conclusion on the ferromagnetic behavior of NiI_2 thin flakes is supported by FORC analysis in Fig. 3. The raw FORC curves and the calculated FORC density diagram $\rho(H_u, H_c)$ are shown in (a) and (b), respectively, at 120 K temperature for the sample from Fig. 2 a. The raw magnetization $M(H, H_r)$ curves confirm ferromagnetic response of the sample. We also ob-

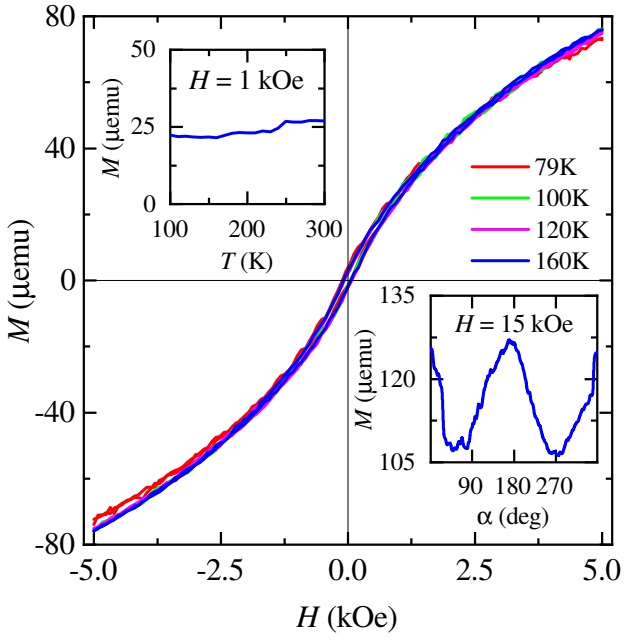

Fig. 4. (Color online) Magnetization loops at 79 K, 100 K, 120 K, 160 K temperatures for the same 18 μm thick, 0.23 mg mass flake as in Fig. 2. We do not see temperature dependence of the ferromagnetic loop within ± 2 kOe field range. $M(T)$ temperature dependence is also weak up to the room temperature, as it is shown in the left inset at fixed 1 kOe field. $M(\alpha)$ angle dependence is shown in the right inset at 160 K temperature for 15 kOe field, it coincides well with the result at 120 K in Fig. 2 *a*

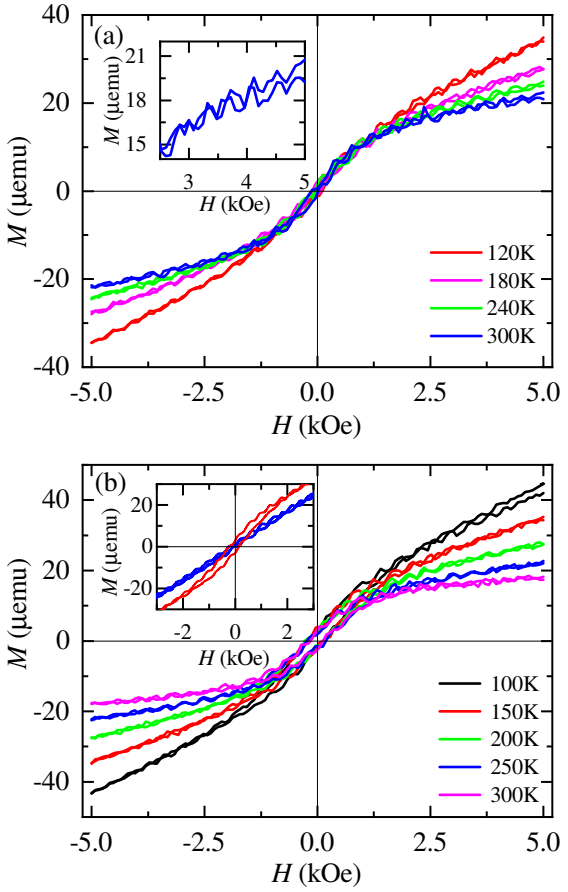

Fig. 5. (Color online) Ferromagnetic hysteresis for a similar (15 μm, 0.20 mg) NiI_2 flake, which is exfoliated after several warmings of the initial crystal to room temperature. *a* — Side mount orientation of the sample, $M(H)$ curves are shown at 120 K, 180 K, 240 K, 300 K temperatures. The hysteresis appears in the same field range ± 2 kOe. However, the saturation level is diminished due to the surface crystallohydrate for thin NiI_2 flakes. Also, temperature dependence is strong above ± 2 kOe, while it is still not present within the hysteresis loop. As an additional result of surface hexahydrate, shallow oscillations appear as modulation of $M(H)$. The oscillations are perfectly reproducible as it is demonstrated in the left inset. *b* — Similar $M(H)$ data for the top mount sample orientation at 100 K, 150 K, 200 K, 300 K temperatures. Magnetic field is within the flake's plane, there is angle dependence of the ferromagnetic hysteresis, as it is shown in the inset for two 120° shifted α values. Similarly to the side mount orientation, the hysteresis loop is not sensitive to temperature within ± 2 kOe field range

serve single peak in $\rho(H_u, H_c)$, which is centered at low H_c values with the so-called open contours at the H_u axis. This behavior is usually regarded as a fingerprint of the multidomain regime for a ferromagnet [27, 28]. The peak center is slightly shifted to the positive values of the interaction field H_u, which corresponds to the dipolar interaction between domains [27, 28].

Ferromagnetic response of NiI_2 thin flakes can be demonstrated at different temperatures, see Fig. 4. The magnetization curves coincide well from 79 K to 160 K, as shown in the main field of Fig. 4. Moreover, the magnetization M value is nearly constant at 1 kOe up to the room temperature, see the left inset to Fig. 4. The angle dependence at 160 K is also identical to one at 120 K, cp. the insets to Fig. 2 *a* and Fig. 4, so there is no sizable temperature dependence for any angle α between the flake surface and the magnetic field for the side-mount orientation of the sample.

We observe qualitatively similar results for different samples, which also allows to highlight an effect of surface degradation due to the crystallohydrate formation. Figure 5 shows magnetization curves for a similar (15 μm, 0.20 mg) flake, which is obtained from the same initial NiI_2 crystal after several warmings to room conditions. Clear ferromagnetic hysteresis can be seen for the side mount and for the top mount flake orientations in (*a*) and (*b*), respectively, for the temperatures

up to 300 K. We also demonstrate typical ferromagnetic anisotropy of magnetization, see the left inset to Fig. 5 *b*. The hysteresis appears in the same field range ±2 kOe, so the coersitivity is independent on the particular sample and on the surface degradation. However, the saturation level is diminished in this case from 80 μemu to 40 μemu for the samples of similar masses (0.23 mg and 0.20 mg, respectively). It seems that the surface crystallohydrate diminishes the $M(H)$ for thin NiI_2 flakes.

Surprisingly, Fig. 5 also shows clear modulation of the magnetization curves by well-reproducible shallow oscillations. We check that there is no oscillations at fixed magnetic field. Some precursors of this behavior can be also seen at low temperatures for the sample from Fig. 4, see the curves obtained at 79 K and 100 K. In Fig. 5, the oscillations can be seen up to 300 K. The oscillations are stronger for the samples, obtained after multiple openings to air, they are well-reproducible and, therefore, requires consistent explanation, as well as the ferromagnetic hysteresis itself.

4. DISCUSSION

As a result, we observe evident ferromagnetic response from thin NiI_2 flakes at temperatures well above the bulk T_{N1}=76 K ordering temperature, while the thick massive flakes show clear paramagnetic signal in this temperature range. If a flake is exposed to air, ferromagnetic hysteresis is accompanied by the periodic modulation of the magnetization curves.

First of all, no magnetic order can be expected [7, 10, 11, 19] above T_{N1}=76 K for bulk NiI_2, which we confirm by clear paramagnetic response for the thick massive flakes in Fig. 2 *c*. We can not completely exclude some crystallohydrate admixture, e.g., while a flake is transferred to the sample holder. However, the NiI_2 crystallohydrate is known to have paramagnetic response [23, 29], so it can not be responsible for the observed ferromagnetic hysteresis.

Bulk NiI_2 is a centrosymmetric magnetic semiconductor, so neither spin-orbit coupling nor the Dzyaloshinskii- Moriya interaction are allowed by the inversion symmetry of NiI_2. Incommensurate spin patterns are also too weak to generate non-negligible Dzyaloshinskii-Moriya interaction [17].

For thin NiI_2 flakes, the situation is more sophisticated due to the anisotropic exchange (Kitaev interaction). Magnetic interactions between localized spins can be generally modeled by the classical spin Hamiltonian, which include the exchange coupling interaction tensors. The latter is generally decomposed into three contributions [13]: the isotropic coupling term, defining the scalar Heisenberg model; the antisymmetric term, which corresponds to the Dzyaloshinskii-Moriya interaction and vanishes in the presence of an inversion center; the anisotropic symmetric term also referred to as a Kitaev term. The latter is expected [13, 17] to determine the helical ground state below T_{N2}. At higher temperatures (above T_{N2}), Kitaev interaction changes antiferromagnetic ground state to ferromagnetic one [20], with strong increase of the ordering temperature T_{N1}. As a result, the monolayer NiI_2 is a ferromagnetic insulator with the calculated T_{N1} about 200 K.

One can expect, that the Kitaev interaction becomes also important for the thin NiI_2 single crystal flakes, which should be a reason to observe magnetic ordering within 80–300 K temperature range, much above the bulk T_{N1}=76 K. As a possible scenario, the above considerations on the Kitaev interaction should be important for the NiI_2 flake surface. The topological spin structures are predicted [13–15] for the NiI_2 surface, e.g. as the spontaneous formation of skyrmionic lattice with a unique, well-defined topology and chirality of the spin texture due to the Kitaev interaction [17]. The surface-defined magnetic response is more important for the thin flakes, which is a good correspondence with our experimental results. Indeed, there is no ferromagnetic response for the massive thick flake in Fig. 2 *c*, while the magnetization saturation level is found to be dependent on the level of surface degradation for the samples of the similar masses, see Figs. 4 and Fig. 5 above ±2 kOe. Also, magnetic anisotropy can be seen for any orientation of NiI_2 flakes, which also correlates with the surface-defined effect.

As about shallow oscillations in Fig. 5, they appear in the experiment if a flake is multiply exposed to air, i.e. for noticeable surface crystallohydrate. On the other hand, shallow oscillations can be expected [31] in the multiferroic state, see also, e.g., Fig.2 in Ref. [32]. Low-symmetric crystallohydrate thin film produces the surface ferroelectric polarization [30] in addition to the described above ferromagnetic properties due to the Kitaev interaction. Thus, the crystallohydrate-affected NiI_2 surface can be considered as artificial multiferroic even at high temperatures.

Multiferroics are materials that exhibit different coexisting ferroic orders such as ferroelectricity, ferromagnetism, or ferroelasticity. Due to the coupling among

the different degrees of freedom leading to these ordered states, the order parameters of one state can be controlled by tuning parameters different from their conjugate variable [33]. In the conditions of our experiment, variation of the magnetic field leads to appearance of the electric field due to the magnetoelectric coupling. Electric field produces mechanical stress in ferroelectrics, which, subsequently, affects magnetization due to the strong magneto-elastic coupling [31]. As a result, variation of the external magnetic field should produce shallow magnetization oscillations.

This mechanism is especially important for a wide band gap semiconductor material NiI_2, with negligible bulk conductivity even at room temperature [34]. Thus, shallow oscillations of magnetization for the crystallohydrate-affected NiI_2 thin flakes should be considered as additional confirmation of the surface origin ferromagnetism in NiI_2.

5. CONCLUSION

As a conclusion, we investigate the magnetic response of thin NiI_2 flakes for temperatures above 80 K. Since no magnetic ordering is expected for bulk NiI_2, we observe clear paramagnetic response for massive NiI_2 single crystals. In contrast, thin NiI_2 flakes show well-defined ferromagnetic hysteresis loop within ± 2 kOe field range. The value of the response does not scale with the sample mass, ferromagnetic hysteresis can be seen for any flake orientation in the external field, so it originates from the sample surface, possibly, due to the anisotropic exchange (Kitaev interaction). The observed ferromagnetism is weakly sensitive to temperature up to 300 K. If a flake is multiply exposed to air, ferromagnetic hysteresis is accompanied by the periodic modulation of the magnetization curves, which is usually a fingerprint of the multiferroic state. While NiI_2 flakes can not be considered as multiferroics above 80 K, surface degradation due to the crystallohydrate formation decreases the symmetry of NiI_2 surface, which produces the surface ferroelectric polarization in addition to the described above ferromagnetic one.

Acknowledgement. We wish to thank S.V. Simonov for X-ray sample characterization.

Funding. We gratefully acknowledge financial support by the Russian Science Foundation, project RSF-23-22-00142, https://rscf.ru/project/23-22-00142/.

REFERENCES

1. Yunye Gao, Mingyuan Gao, and Yuerui Lu, Nanoscale **13**, 19324 (2021).
2. Wei Sun, Wenxuan Wang, Hang Li, Guangbiao Zhang, Dong Chen, Jianli Wang, and Zhenxiang Cheng, Nature Comm. **11**, 5930 (2020).
3. Liemao Cao, Xiaohui Deng, Guanghui Zhou, Shi-Jun Liang, Chuong V. Nguyen, L. K. Ang, and Yee Sin Ang, Phys. Rev. B **105**, 165302 (2022).
4. J. Soödequist and T. Olsen, 2D Materials **10**, 035016 (2023).
5. Shuqing Zhang, Fawei Tang, Xiaoyan Song, and Xinping Zhang, Phys. Rev. B **105**, 104105 (2022).
6. T. Kurumaji, S. Seki, S. Ishiwata, H. Murakawa, Y. Tokunaga, Y. Kaneko, and Y. Tokura, Phys. Rev. Lett. **106**, 167206 (2011).
7. T. Kurumaji, S. Seki, S. Ishiwata, H. Murakawa, Y. Kaneko, and Y. Tokura, Phys. Rev. B **87**, 1 (2013).
8. Hwiin Ju, Youjin Lee, Kwang-Tak Kim, In Hyeok Choi, Chang Jae Roh, Suhan Son, Pyeongjae Park, Jae Ha Kim, Taek Sun Jung, Jae Hoon Kim, Kee Hoon Kim, Je-Geun Park, and Jong Seok Lee, Nano Lett. **21**, 5126 (2021).
9. D. Khomskii, Physics **2**, 20 (2009).
10. S. R. Kuindersma, J. P. Sanchez, and C. Haas, Physica B **111**, 231 (1981).
11. D. Billerey, C. Terrier, N. Ciret, and J. Kleinclauss, Phys. Lett. A **61**, 138 (1977).
12. Q. Song, C. A. Occhialini, . Ergecen, B. Ilyas, D. Amoroso, P. Barone, J. Kapeghian, K. Watanabe, T. Taniguchi, A. S. Botana, S. Picozzi, N. Gedik, and R. Comin, Nature **602**, 601 (2022); doi:10.1038/s41586-021-04337-x.
13. D. Amoroso, P. Barone, and S. Picozzi, Nature Comm. **11**, 5784 (2020); doi:10.1038/s41467-020-19535-w.
14. K. Riedl, D. Amoroso, S. Backes, A. Razpopov, Thi Phuong Thao Nguyen, K. Yamauchi, P. Barone, S. M. Winter, S. Picozzi, and R. Valentí, Phys. Rev. B **106**, 035156 (2022).
15. Feng Lou, X. Y. Li, J. Y. Ji, H. Y. Yu, J. S. Feng, X. G. Gong, and H. J. Xiang, J. Chem. Phys. **154**, 114103 (2021).
16. Jinyang Ni, Xueyang Li, Danila Amoroso, Xu He, Junsheng Feng, Erjun Kan, Silvia Picozzi, and Hongjun Xiang, Phys. Rev. Lett. **127**, 247204 (2021).

17. Xuanyi Li, Changsong Xu, Boyu Liu, Xueyang Li, L. Bellaiche, and Hongjun Xiang, arXiv:2211.14416v2 (2023).

18. D. Lebedev, J. T. Gish, E. S. Garvey, T. Kh. Stanev, J. Choi, L. Georgopoulos, Th. W. Song, H. Y. Park, K. Watanabe, T. Taniguchi, N. P. Stern, V. K. Sangwan, and M. Ch. Hersam, Adv. Funct. Mater. **33**, 2212568 (2023).

19. I. Melchakova, E. A. Kovaleva, N. S. Mikhaleva, F. N. Tomilin, S. G. Ovchinnikov, A. A. Kuzubov, P. Avramov, Int. J. Quant. Chem. **120**, 243001 (2019).

20. A. S. Botana and M. R. Norman, Phys. Rev. Materials B **3**, 044001 (2019).

21. Vadym V. Kulish and Wei Huang, J. Mater. Chem. C, 5, 8734 (2017); doi:10.1039/C7TC02664A.

22. A. H. M. Abdul Wasey Debjani Karmakar and G. P. Das, J. Phys.: Cond. Matter **25**, 476001 (2013); doi:10.1088/0953-8984/25/47/476001.

23. M. Louër, D. Grandjean, and D. Weigel, J. Sol. St. Chem. **7**, 222 (1973).

24. M. A. McGuire, Crystals **7**, 121 (2017); doi:10.3390/cryst7050121.

25. B. C. Dodrill, *Magnetometry Measurements and First-Order-Reversal-Curve (FORC) Analysis*, Lake Shore Cryotronics, www.lakeshore.com.

26. D. A. Gilbert, P. D. Murray, J. De Rojas, R. K. Dumas, J. E. Davies, and K. Liu, Sci. Reps. **11**, 4018 (2021).

27. B. C. Dodrill, H. S. Reichard, and T. Shimizu, *Lake Shore Cryotronics. Technical Note*, www.lakeshore.com.

28. B. C. Dodrill, *Magnetometry Measurements of Nanomagnetic Materials, Advanced Materials: ThechConnect Briefs*, www.lakeshore.com.

29. S. M. Abozeid, E. M. Snyder, A. P. Lopez, C. M. Steuerwald, E. Sylvester, K. M. Ibrahim, R. R. Zaky, H. M. Abou-El-Nadar, and J. R. Morrow, Eur. J. Inorg. Chem. 1902 (2018); doi:10.1002/ejic.201800021.

30. F. Cariati, F. Masserano, M. Martini, and G. Spinolo, J. Raman Spectr. **20**, 773 (1989).

31. V. Gunawan and Ngurah Ayu Ketut Umiati, Int. J. Electr. Comp. Engin. (IJECE) **8**, 4823 (2018); doi:10.11591/ijece.v8i6.

32. G. Cardenas-Chirivi, K. Vega-Bustos, H. Rojas-Páez, D. Silvera-Vega, J. Pazos, O. Herrera, M.A. Macías, C. Espejo, W. López-Pérez, J. A. Galvis, ad P. Giraldo-Gallo, arXiv:2212.02490.

33. A. O. Fumega and J. L. Lado, 2D Materials **9**, 025010 (2022); doi:10.1088/2053-1583/ac4e9d.

34. D. Lebedev, . T. Gish, E. S. Garvey, T. Kosev Stanev, Junhwan Choi, L. Georgopoulos, T. W. Song, Hong Youl Park, K. Watanabe, T. Taniguchi, N. P. Stern, V. K. Sangwan, and M. C. Hersam, Adv. Funct. Mater. **33**, 2212568 (2023).